Temperature Microstructure in the Equatorial Atlantic

T. R. OSBORN AND L. E. BILODEAU[1]

Institute of Oceanography, University of British Columbia, Vancouver, B.C., Canada V6T 1W5

(Manuscript received 6 November 1978, in final form 3 July 1979)

ABSTRACT

Vertical profiles of temperature microstructure were collected at seven sites in the equatorial Atlantic between 24°W and 33°W, 2°N and 1°20'S. The use of three identical temperature microstructure profiles gives insight into the spatial and temporal variation of the temperature microstructure. Data on the velocity microstructure taken with a fourth instrument show a relationship between temperature and velocity microstructure.

Cox numbers show a relative minimum near the center of the core with largest values in the shear region between the South Equatorial Current and the Equatorial Undercurrent.

1. Introduction

Small-scale temperature fluctuations have been studied in recent years in an attempt to gather some insight into the mixing processes that are active in the ocean. Gregg *et al.* (1973) and Gregg (1977) have found the temperature gradient variance arises essentially from scales smaller than 0.5 m. Temperature structure at these scales is now usually called microstructure. Numerical estimates for vertical heat flux and eddy coefficients can be derived using the model of Osborn and Cox (1972). This model retains only the mean vertical gradient and the gradient variance as relevant parameters, and incorporates simplifying assumptions such as horizontal homogeneity and steady state, whose importance have never been assessed. In spite of these shortcomings the scaling of the model, which is mean-square temperature gradient divided by the mean gradient squared (the Cox number) has become a standard parameter for describing microstructure.

The work of Gregg and Cox (1971) and later Gregg (1977) on measuring the small-scale density fluctuations has given insight into the microstructure in the ocean. The relative contributions of the different mechanisms responsible for ocean microstructure are still unknown. Small-scale density inversions in generally stable regions are suggestive of overturns such as shown in the pictures of Woods (1968) and in extensive studies by Thorpe (1971). The breaking of internal waves generated by shear instability is considered a likely source. The pictures of Woods show this process occurring in the thermocline off Malta. Direct extraction of turbulent energy from the mean shear has been suggested by Crawford and Osborn (1979b) in the shear zone above the Atlantic Equatorial Undercurrent, and by Osborn (1978) in the thermocline adjacent to the Azores. Gargett (1976) presents statistical evidence for the importance of salt fingering on local regions as a mechanism for turbulent mixing. Gregg and Cox (1971) showed profiles indicating probable double diffusion sites.

This paper reports on temperature microstructure measurements taken in the equatorial Atlantic during June and July 1974 from the *Atlantis* II. [See Bruce and Katz (1976) for a complete description of the hydrographic conditions.] Three identical instruments were used to profile temperature and temperature gradient. A fourth probe measured temperature and velocity microstructure simultaneously. The velocity microstructure data and the details of their conversion to estimates of the local rate of viscous energy dissipation are described in Crawford and Osborn (1979a). Portions of those data are used in this paper to qualitatively show the relationship between temperature and velocity microstructure as well as the variation in turbulence with depth and location. This paper also looks at the size scales (vertical and horizontal) and the time scales of the turbulent features using the simultaneous and/or repeated temperature microstructure data augmented with the energy dissipation data. Recent developments in the understanding of the frequency response of thermistors (Lueck *et al.*, 1977) allow us to correct the data and to present Cox number estimates. Eventually one must determine the size and lifetime of the microstructure patches to perhaps shed some light on the generating mecha-

[1] Present affiliation: Hydro Québec, Etudes et avant-projets, Montréal, Québec.

0022-3670/80/010066-17$08.25

nisms. This task is complicated by the irregular shape and differential motion in the water column. However, these data do show some interesting features and the data processing procedure is designed to facilitate the comparison of finestructure and microstructure features between drops. Finally, there are some interesting comparisons with Gregg's (1976) measurements in the Pacific Equatorial Undercurrent.

2. Instrumentation and data analysis

Most of the data were collected with three small identical instruments called "Pumpkins" because of the red plastic flotation sphere (see Fig. 1). The temperature was sensed by a microbead thermistor located on the lower end. The signal was fed to a set of electronics that produced two FM signals, one proportional to the temperature and the other proportional to its time derivative. These signals were telemetered to the surface with a Sippican Expendable Wire Link (XWL). The data were recorded on 0.25 inch magnetic tape for later analysis and were displayed on chart paper for real-time monitoring. For the Pumpkins, fallspeed was estimated from calibration drops using a special set of electronics with a pressure transducer instead of temperature sensing electronics. The Pumpkins were designed to be small and as simple as possible to operate in order to facilitate the shipboard operations, hence no pressure transducer was included in the basic electronics. The instruments are described in more detail in Osborn (1977) and the thermistor response problem is discussed in Lueck *et al.* (1977).

Data were also collected with a large free-fall instrument called the "Camel" which measured pressure, temperature and its time derivative and velocity shear. Those data are used to produce profiles of temperature, its gradient and energy dissipation. Although the electronics are similar to that of the Pumpkins, the fallspeed is about twice as fast (0.4 m s^{-1} as compared to the Pumpkin's nominal value of 0.2 m s^{-1}). For more details on the measurements with the Camel see Crawford and Osborn (1979a) and Osborn (1977).

The first step in the analysis of the temperature data consisted of digitizing the data at a rate of 250 Hz for the Pumpkins. The Camel data were digitized for another project generally at a rate of 200 Hz. After digitizing, the data were examined for bad points and these were removed and replaced by appropriate values. The temperature was then plotted as a function of depth using the nominal fallspeed in the case of the Pumpkins or the pressure record in the case of the Camel. Temperature calibration data used for this came from measurements made whenever a thermistor was changed. The individual frequency responses of the thermistors were not measured.

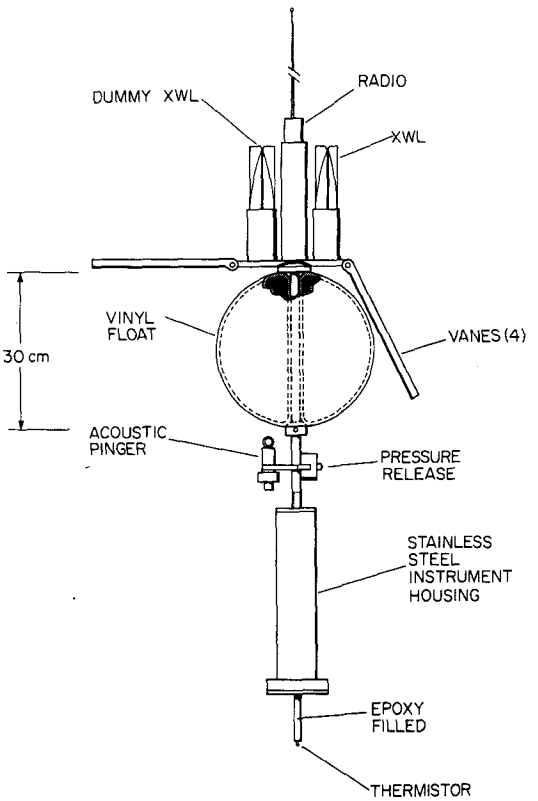

FIG. 1. Schematic drawing of the Pumpkin.

For each station that will be considered in this paper there are at least two profiles. Due to differences in the nominal fallspeeds the raw data are not easily compared. Comparison with the STD records showed differences in the temperature up to 0.5°C that were believed to be due to systematic errors. Therefore, to bring all the data at a given station to comparable depths and align the same features between drops, the depth and temperature scales were adjusted. The technique used was as follows. First, one of the free-fall profiles was adjusted in both temperature and depth for a best fit by eye with the STD data provided by Dr. Eli Katz of WHOI. These STD data were taken at the same nominal location as the microstructure data, usually within a few hours. Both the temperature and depth scales were adjusted in a linear fashion. This adjustment corresponds to no more than a zero shift and a gain (or fallspeed) change. After one profile has been fitted to the STD data, all the other profiles obtained at the same station were fitted to the first profile. The reason for fitting to the free-fall profile rather than fitting to the STD data is that the free-falls occur relatively close in time and space and are more self-similar. Due to the large number of similar finestructure features in the temperature profiles,

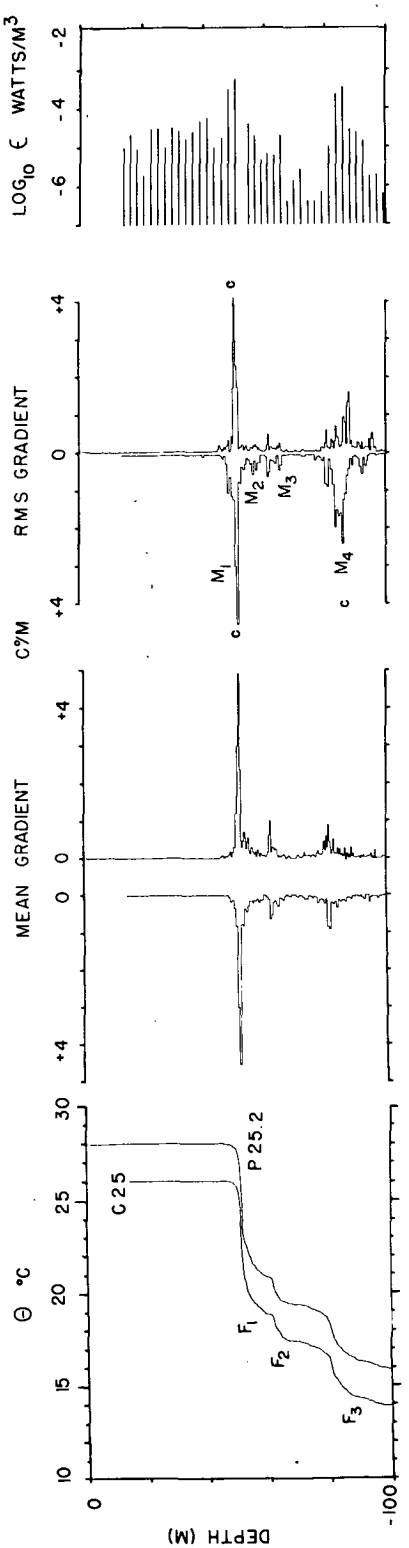

FIG. 2. Drop 25 Pumpkin and Camel plots of mean temperature, mean gradient and rms gradient. Only the T profiles are labeled as to instrument and drop number. The other profiles are in the same order.

this comparison procedure is fairly simple and the results seem quite satisfactory. The Pumpkin depths were stretched by 3–11%. The Camel depths were generally changed 3% or less. While this procedure may seem drastic, the finestructure features will be seen to correspond well between profiles. The analysis emphasizes the similarity of prominent features in the profile while showing spatial and temporal variations (see Fig. 2).

The temperature derivative data are used in two different ways. First, the vertically averaged temperature gradient is calculated in blocks of 512 digitized points. This corresponds to just slightly more than 2 s, or vertical intervals of ~0.4 m for the Pumpkins at their nominal fall-speed of 0.2 m s^{-1}. For the Camel the averaging depth interval is almost 1 m. Second, the root-mean-square (rms) temperature gradient is calculated over the same interval. The rms gradient is calculated relative to the mean gradient over the interval

$$\left(\frac{\partial\theta}{\partial z}\right)_{\text{rms}} = \left[\overline{\left(\frac{\partial\theta}{\partial z} - \frac{\overline{\partial\theta}}{\partial z}\right)^2}\right]^{1/2},$$

where the overbar denotes averaging over the block of 512 digitized points. The Osborn-Cox model retains the variance of the temperature gradient as a significant parameter rather than its square roots. Plotting the rms gradient allowed small intensity patches to show up more than in variance profiles. The value of the mean temperature gradient is accurate to ±10%. It is calibrated against the mean temperature profile. The uncertainty in gradient is due to uncertainties in the depth and temperature scales. The rms gradient has the same uncertainty plus the problem of limited sensor frequency response which reduces the value of the measured rms gradient. Lueck *et al.* indicate that the response of our thermistors, at the speeds of the Pumpkins, are down at least 3 dB at a vertical scale of 15 mm. The resolution is comparable to that of Gregg's (1976) measurements in the Pacific. For the temperature gradient measurements with the Camel the fallspeed is twice as large and the spatial resolution is considerably poorer, with the −3 dB point at scales on the order of 30 mm. Because of the poorer spatial resolution the Camel rms temperature gradient values are consulted for qualitative rather than quantitative results.

These data are then plotted as profiles, with data from each drop or associated drops being put on the same plot for easy comparison. All the averaged profiles are plotted in a similar fashion. On the left are the mean temperature traces which are labeled as to drop and instrument number. For example, C28 is Camel drop 28. P19.3 is Pumpkin 3, drop 19. To the right of the mean temperature profiles are

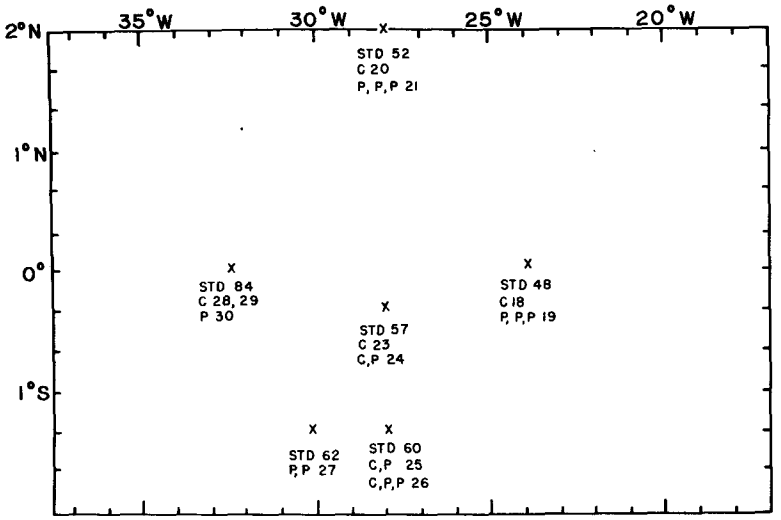

FIG. 3. Locations of the drops, in which both Camel and Pumpkin data are available. C indicates a Camel drop and P a Pumpkin drop; C, P, P indicates a Camel plus 2 Pumpkins.

the average gradient profiles in the same order as the temperature profiles. Hence, the drop numbers are not labeled on the gradient traces. Next the rms gradients are plotted in the same order. Finally the relevant dissipation profiles are plotted. The traces all show a great deal of similarity. The vertically averaged gradient and rms gradient data are plotted like an inkblot diagram to make comparisons easier. This technique is always possible for the rms gradient which is positive definite, and works well on this data set because the mean gradient has so few reversals that the traces do not get confused.

The above analysis procedure is designed to allow us to identify and compare both the finestructure and microstructures of the records. The summary of the data produced in this fashion still needs to be supplemented with detailed examination of the original, non-averaged data records. The calibration and alignment used in the above procedure are also applied to the original data traces making them easier to intercompare. Therefore, as we examine the data we will use both the summarized data format and the original traces to examine the nature of the microstructure.

Using the results of Lueck *et al.* (1977) it is possible to correct spectrally the temperature gradient variances for the attenuation of the thermistor. Corrections for the thermistor are derived by Lueck (personal communication) assuming a boundary-layer scaling proportional to $U^{1/3}$ and that the thermistors' parameters are the same as similar thermistors they tested. Based on our knowledge of the thermistor response scaling, we feel this correction is the most suitable one. If the scaling is not correct, then the values of the variance reported here are more likely to be underestimates than overestimates since the $U^{1/2}$ scaling would increase the correction factor. The electronics are accounted for from the nominal values of the circuit parameters. Variances of the temperature gradient are calculated over depth intervals where the regions are relatively uniform in terms of mean gradient.

Full scale of the temperature gradient circuits on the Pumpkin was ~ 17.5 C° m^{-1} (it varies between instruments and with fall-speed). Thus in regions where the instantaneous gradient exceeds the full-scale value the signal saturates and the peak gradients are clipped. For the plots of the mean gradient and the rms gradient the effect is to lower the values in those regions where the signal is clipped. Such regions are marked on the plots with a C to indicate clipping. Regions in which the Camel data are clipped are also indicated. Clipping of the peak data values affects the spectral representation in two ways. First, it reduces the total variance and second it redistributes the variance among the frequencies. Since the correction for the thermistor attenuation is a monotonically increasing function of frequency, a redistribution of the variance can affect the validity of the correction scheme. In order to minimize the effects of the clipping, only data where a few points saturated at a time were used—generally, one to three points but once as many as six points in a row. Thus, for example, profiles from the Pumpkins on drop 26 were not used. In an attempt to estimate the effect of limiting the peak values, the data that were corrected for thermistor response were clipped at lower levels (± 400 and ± 450 units versus the original ± 511 units). The variance was found to be lower by 4–10% with a slight redistribution in the contribu-

tions as a function of frequency. From this test it is felt that the effect of the clipping in the results reported is to decrease the variance so that the values shown are a lower bound. Since the drops through the Undercurrent show less saturation due to the spreading of the mean temperature gradient, most of these drops were usable.

3. Data

Fig. 3 shows the location of the different data producing drops. Each drop consists of one or more instruments released at relatively close intervals of time and space. Consecutive drops of the same instrument—which require a time spacing of ~1 h to allow for recovery of the first instrument—or consecutive drops of different sets of instruments, are given different drop numbers. Table 1 contains information about the location and timing of launch and recovery.

The profiles can be put into three natural groupings by their relation to the Equatorial Undercurrent. Drops 25, 26 and 27 are all south of the southern edge of the current, drops 18, 19, 23, 24, 28, 29 and 30 are through or near the core of the current, and drops 20 and 21 are to the north of the current. The easiest place to start is with the most southerly data, then we will look at the data north of the Equatorial Undercurrent, and finally the data showing the Undercurrent.

a. Drops 25, 26 and 27

Drops 25 and 26 were taken 1.5 h apart at the same nominal location. Drop 27 was taken 120 n mi further west but at essentially the same latitude (1°20′S).

The data from drop 25 are shown in Fig. 2 as an example of the results of the analysis procedure. Fig. 4 shows the original temperature and temperature gradient traces for drop 25 so that the following discussion can be compared to the original data. This drop consisted of one Pumpkin and the Camel operated in unison, with the Pumpkin released 2 min before the Camel. The two instruments reached the thermocline at almost the same

TABLE 1. Details of the launch and recovery of the drops. The recovery column indicates the relative position of the instruments on their return to the surface.

Drop	Instrument type and number		Launch	Date	Recovery
18	C	24°00′W 0°02′N	1332	10 July	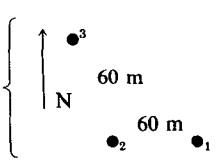
19	P_1		1449	10 July	
	P_2		1450	10 July	
	P_3		1451.5	10 July	
20	C	28°11′W 2°9′N	1325 side of ship	14 July	
21	P_1		1433 side of ship	14 July	
	P_2		1437 side of ship	14 July	
	P_3		1437 stern of ship	14 July	
23	C	28°01′W 0°18′S	1322	16 July	
24	P	28°03′W 0°17′S	1438 1431	16 July 16 July	no information
25	P_2	28°03′W 1°21′S	120 s apart Pumpkin then Camel	17 July	30 m apart
26	P P_3 C		Pumpkins simultaneously 15 m apart, Camel 3 min later	17 July	Pumpkins 15 m apart, Camel 50 m away to the north
27	P_1 P_3	30°02′W 1°20′S	Ship steaming north about 3 kt, released 2 min later	18 July	About 200 m apart on north-south line
28	C	32°59′W 0°23′N	0917	23 July	
29	C		1020	23 July	
30	P_3	33°W 03′N	1100	23 July	

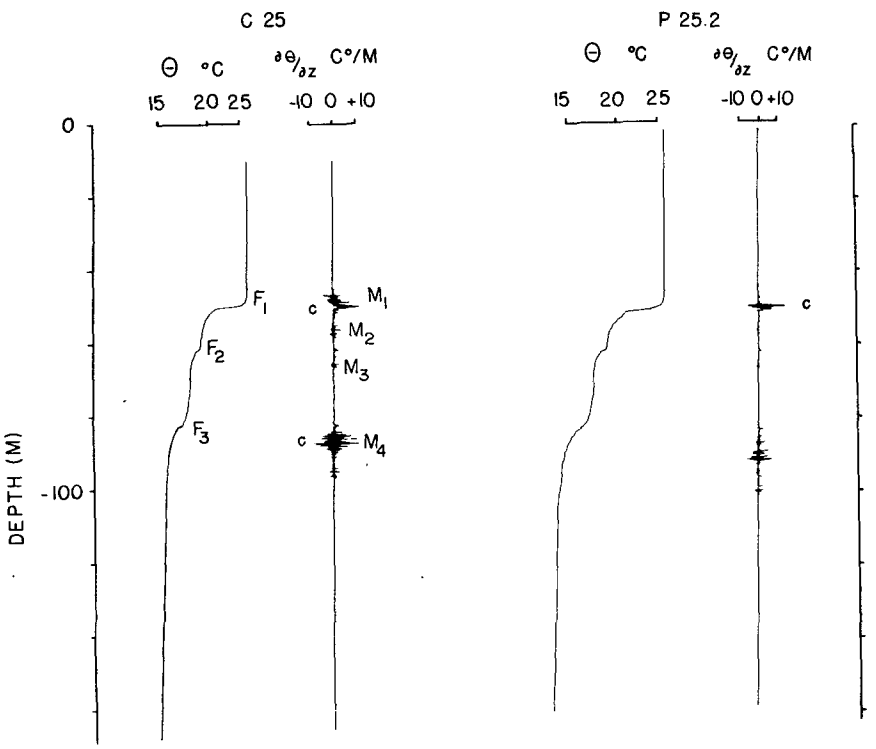

FIG. 4. Original data from drop 25.

time and the Pumpkin was 100 s later than the Camel at 100 m depth. An examination of Fig. 2 shows how similar the two temperature traces are, which is essentially the justification for the analysis procedure of aligning the depth traces by using the temperature features. Three distinct temperature finestructure features have been labeled F_1, F_2 and F_3; these features are the thermocline at 50 m depth and two temperature decreases located at 70 and 80 m depth. These finestructure features show up well in the mean gradient profile.

The rms gradient profiles show large contributions from the region of the thermocline (labeled M_1) and below the finestructure feature near 80 m depth (labeled M_4). The original data of Fig. 4 show that the large rms gradient in the upper edge of the thermocline (M_1) is composed of small-scale gradient fluctuations as well as a contribution from the large mean gradient. Comparison of the rms gradient plot with the dissipation profiles shows that a relative peak in the dissipation at the upper edge of the thermocline is associated with patch M_1. In the region below 80 m there is also a high dissipation layer associated with patch M_4. Near 60 m depth, dissipation values are 10 times smaller than the peak values at the other levels and the same is true of the gradient variance of patches near M_2 and M_3.

The rms gradient patches M_1 and M_4 are located in the vicinity of finestructure features F_1 and F_3. Notice, however, that both microstructure patches are located either just above or just below the layer of highest mean gradient, but not on it. Any relationship is unclear in the case of features F_2, M_2 and M_3.

On Fig. 4, the temperature finestructure feature at 60 m depth appears as a broad, quite one-sided temperature decrease in both profiles. There is a small amount of microstructure (labeled M_3) below it that shows up as a peak in the rms profile of the Camel. This patch is about 1 m thick and about the same height as the rms value for the temperature decrease. As mentioned before, the analysis procedure calculates the rms gradient by subtracting the mean value of each block from each value, squaring the values and summing the values over the block. Thus the feature at 60 m depth shows in the rms profile partly because the values of the mean gradient varies over the feature.

There are microstructure patches (labeled M_2) in both traces between the thermocline and the first finestructure patch. The rms gradient is larger in the Camel trace.

For drop 26 there are data from the Camel and two Pumpkins but no dissipation estimate could be made (Figs. 5 and 6). The Camel was released last and the Pumpkins 3 min earlier, one from the stern and the other from amidships. Thus the Pumpkin reached the thermocline 1 min before the

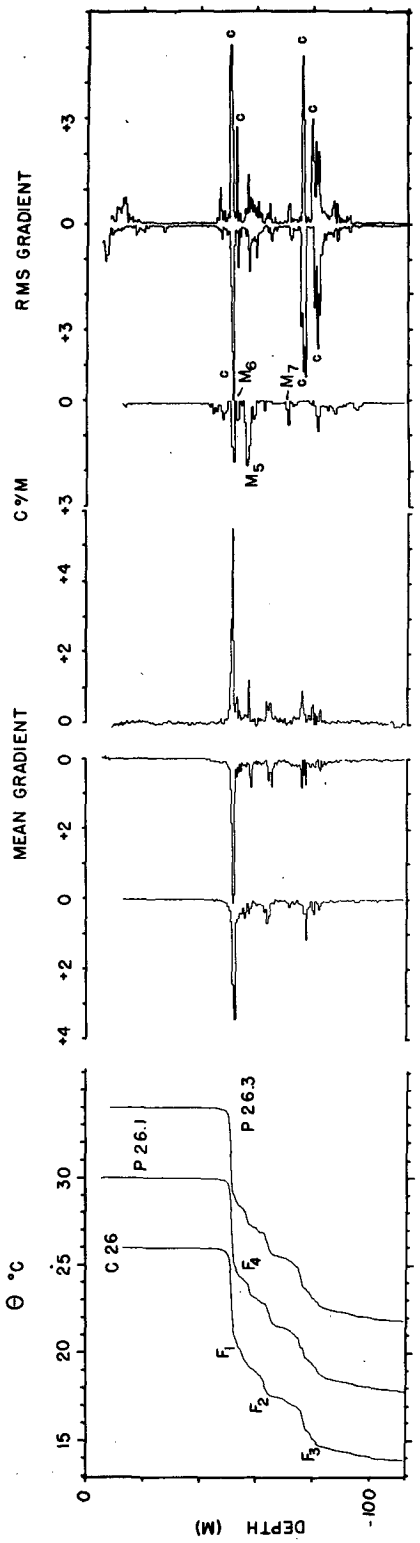

FIG. 5. Drop 26 processed data.

Camel and 100 m 1 min after the Camel. The Camel temperature profile is similar to that of drop 25, the middle finestructure feature (F_2) is ~2 m deeper and F_3 is ~5 m shallower. The Pumpkins show another finestructure just below the thermocline at ~58 m depth for which there is no comparable feature in the Camel or either trace from drop 25. This feature is quite visible in the mean gradient profiles of the Pumpkins (labeled F_4) while there is a strong feature at the corresponding level in the Camel's rms gradient profile (labeled M_5).

When examining the Pumpkin traces, an outstanding feature is the change in the microstructure associated with the bottom finestructure feature F_3. The microstructure near 75–80 m is now concentrated into two patches. In the Pumpkin profiles, the upper microstructure patch (75 m) is situated right where most of the temperature change takes place. Pumpkin 1 reveals that this temperature change presents two steps separated by a thin well-mixed but very active region (the mean gradient profile of P26.1 shows a double peak at 75 m). The lower patch also coincides with a region of temperature decrease, the bottom part of which appears to have temperature microstructure in the Camel profile also. The intensity of this patch is lower in profile C26 than in C25 while it is higher in P26.1 and P26.3 than in P25.2.

There is a microstructure patch right in the thermocline (the base of the mixed layer). In the original data, this is associated with one-sided gradient pulses of high amplitude. Just above and below, one can see smaller amplitude gradient fluctuations where the gradient takes both signs. About 2 m below the thermocline there is a microstructure feature in all three traces which shows particularly well in Fig. 6 (M_6). The patch below that (M_5) is also seen in all three traces at this location. In the Pumpkin traces, it is accompanied by a temperature step which, as noted before, does not appear in the Camel data. This microstructure patch could be continuous with M_2 on drop 25. The finestructure feature that corresponds to F_2 in drop 25 is of the same nature as F_2 in drop 26. Its gradient signal is also one-sided (and nonturbulent). The thin feature labeled M_7 appears in all three traces.

Drop 27 consists of a pair of Pumpkin traces and is included because it is from nominally the same type of environment as drops 25 and 26. Examination of the plot (Fig. 7) shows that the finestructure is somewhat simplified. Here, only two large temperature steps account for most of the temperature change between 50 and 100 m. The rms gradient is at a lower level than in the previous drops. Another noticeable feature is a patch of microstructure at ~58 m depth that exists only in one of the profiles (M_8). Examination of the original

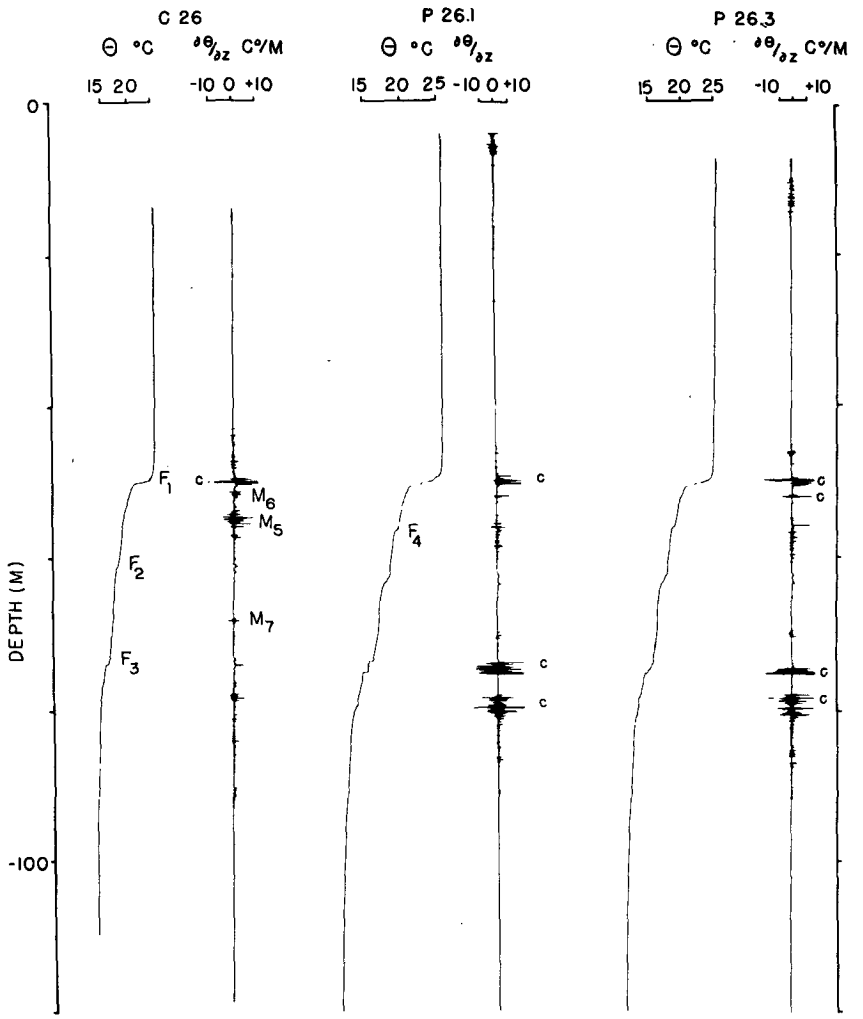

FIG. 6. Original data from drop 26.

data traces shows them to be very similar except for this feature which appears only in one trace.

The important features in drops 25, 26, and 27 are as follows:

1) The basic temperature profile is consistent between drops 25 and 26 with the addition of one finestructure feature in the two Pumpkin profiles of drop 26.

2) There is an active patch just above the thermocline (in the bottom part of the mixed layer or upper edge of the thermocline). The intensity varies between samplings. This temperature microstructure is associated with a relative peak in the energy dissipation for Camel 25.

3) In drops 25 and 26 there is microstructure below F_3 associated with a relative peak in the dissipation. This microstructure appears to change in time and location as does the interface itself.

4) Drop 27 is grossly similar to the other two drops in terms of the temperature profile but quantitative levels of the mean and rms gradients are smaller.

5) The major microstructure features seem to extend in time and space between instruments and drops. However, levels and details can change.

b. Drops 20 and 21

We now turn our attention to profiles obtained at 2°N and thus north of the Equatorial Undercurrent. Fig. 8 shows drop 20, which was a Camel profile, and drop 21, consisting of 3 Pumpkins 1 h later. Pumpkin 3 had a problem with the zero level of the gradient channel and while those data are usable for an rms value (without the mean removed), the mean gradient is too severely affected to use with our analysis procedure (and is not presented in Fig. 8). The three Pumpkin rms gradient profiles are similar in shape. Pumpkin 3 also shows a

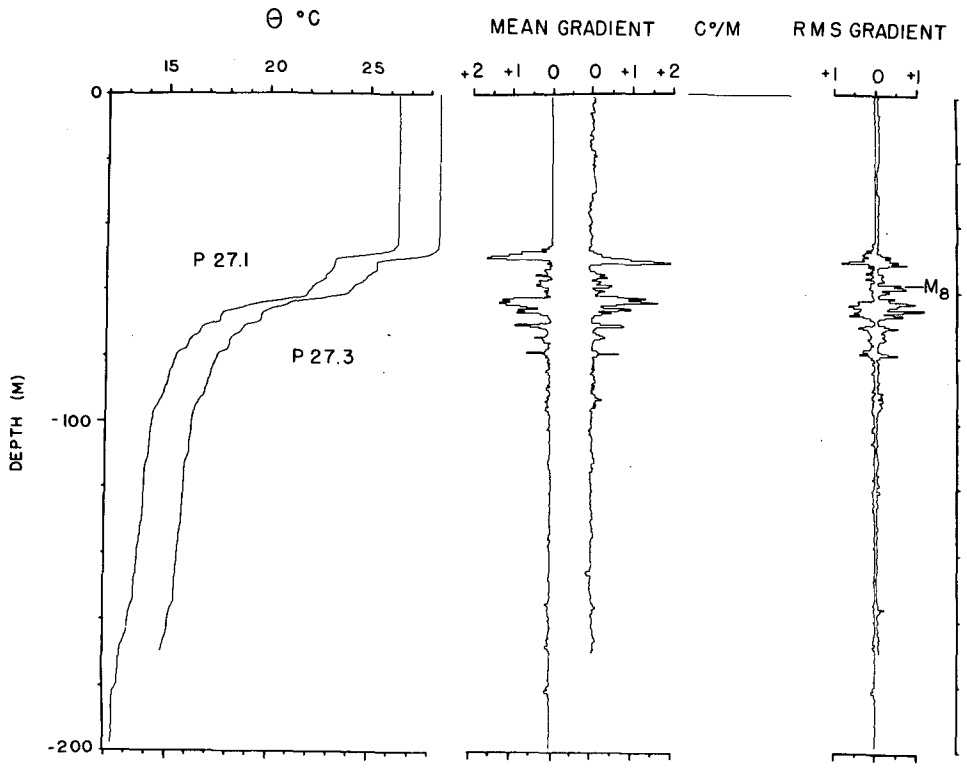

FIG. 7. Drop 27 processed data show temperature, mean gradient and rms gradient.

strong patch of activity near 25 m depth in the upper layer. Examination of the original data trace indicates that this is not due to instrumental problems, although it might possibly be contamination due to the presence of the ship's hull. Much of their gradient variance is associated with the finestructure features below the thermocline. The upper layer is not as uniform as in drops 25 and 26 (south of the equator). The Pumpkins all show a small amount of microstructure at 50 m depth which is the base of the upper layer. The most interesting feature in these profiles is the change between the Camel drop and the Pumpkins' in the 70–90 m range. The Pumpkins show two isothermal patches and a temperature step labeled F_5 which does not appear in the Camel trace. The Camel data in this region show a large amount of microstructure (M_8) and a relatively large local rate of energy dissipation. The Pumpkins show a number of thin, high amplitude rms gradient patches. Differences are also found in the 50–70 m range where the Camel shows three thin layers of microstructure (labeled M_9) and the Pumpkins show one large feature at the bottom. The thin microstructure feature just above 100 m depth in the Camel trace does not appear in the Pumpkin data. The rms gradient patches from the Camel coincide with the relative maximums of energy dissipation even near 40 m where the mean gradient is so small that not much rms is noticed.

The important features in drops 20 and 21 are as follows:

1) The strong similarity between the Pumpkins launched at the same time with a separation of 15 m. Pumpkin 3 launched 4 min later shows less similarity in the details although the general location and intensity of the microstructure is the same (except for the active patch in the mixed layer).

2) The difference in the region from 75 to 87 m depth between the Camel profile and the Pumpkin profiles which were taken about one hour apart.

c. Undercurrent profiles

We now turn to the data collected through the Equatorial Undercurrent. Drops 18 and 19 (Fig. 9) were on the equator near 24°W. The measurements of Bruce and Katz (1976) indicate the core of the current was 20′ south of the equator at that longitude and time. Drops 23 and 24 (Fig. 10) were taken ~2 mi apart at 18′S, 28°02′W through the salinity core of the Undercurrent according to the cross sections of Bruce and Katz. Drops 28, 29 and 30 (Fig. 11) were almost centered on the equator at 33°W, through the center of the Undercurrent. In all of these drops we see the classic spreading of the thermocline associated with the Undercurrent. There is a region of microstructure associated with relatively high dissipation in the upper edge above

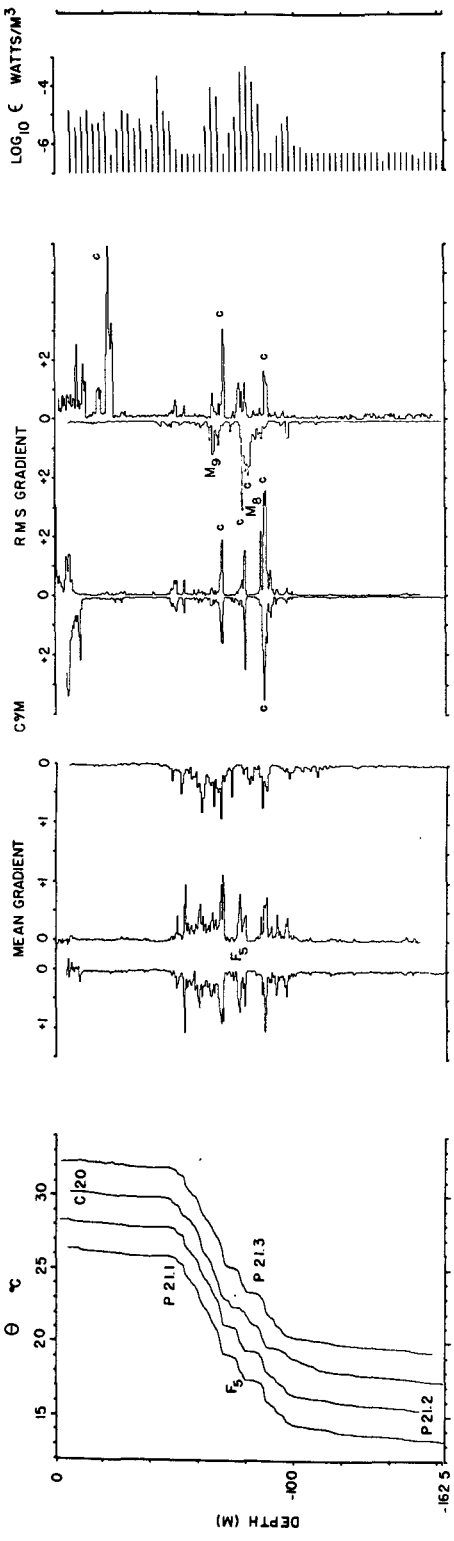

FIG. 8. Processed data from drops 20 and 21. Although the Camel was dropped first it is plotted as the third in the series so that Pumpkins 21.1 and 21.2 can be plotted back to back.

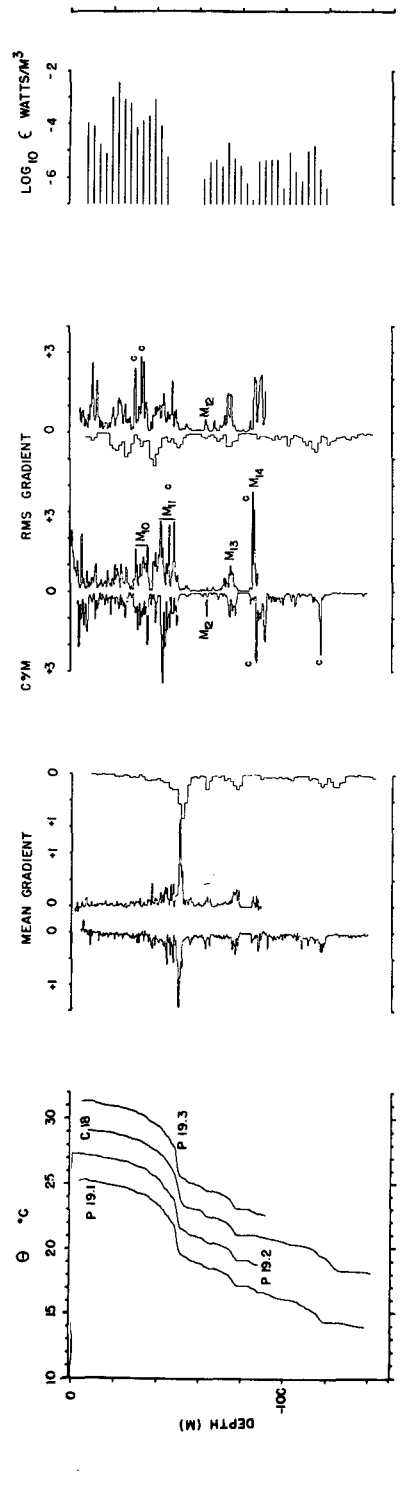

FIG. 9. Drops 18 and 19 processed data. A slower digitizing rate on the Camel leads to a greater averaging interval and hence lower values of mean gradient and rms gradient. There is no mean gradient traces for P19.3 (see text).

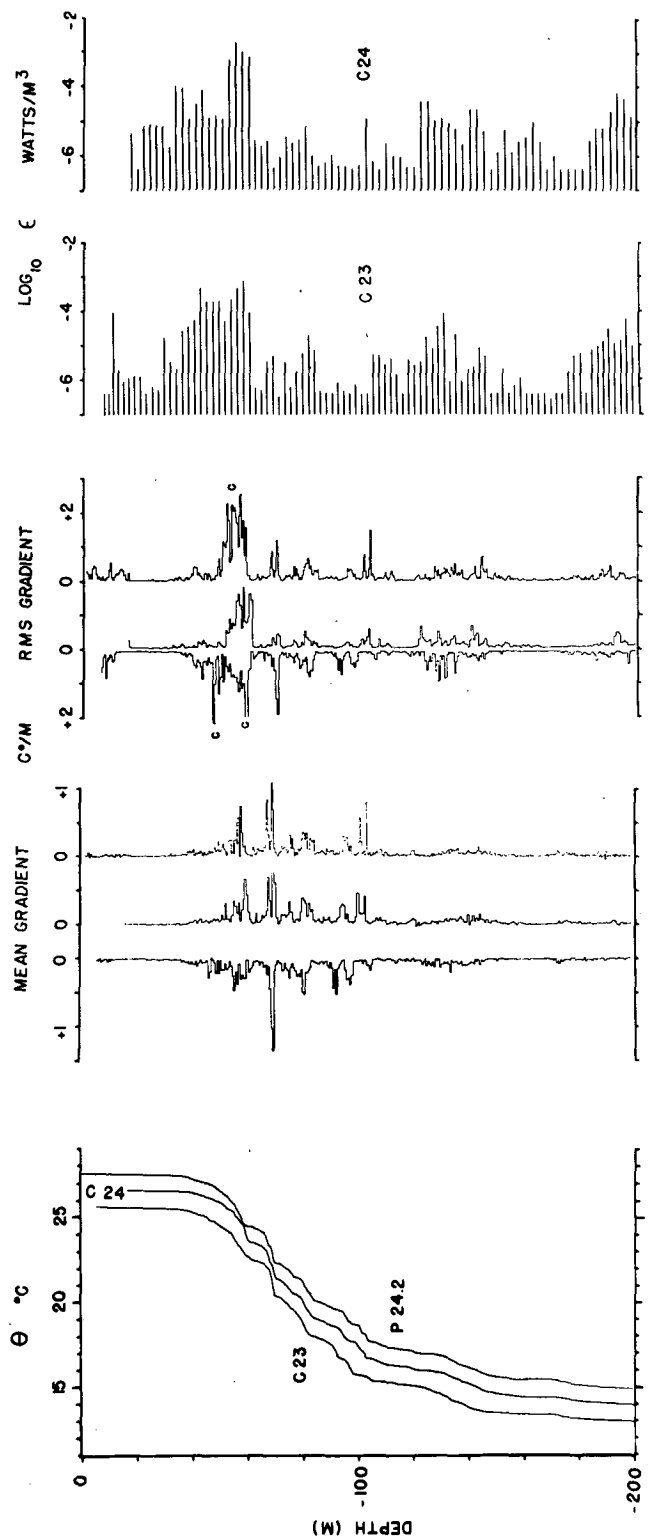

FIG. 10. Camel drop 23, Camel drop 24 and Pumpkin drop 24.

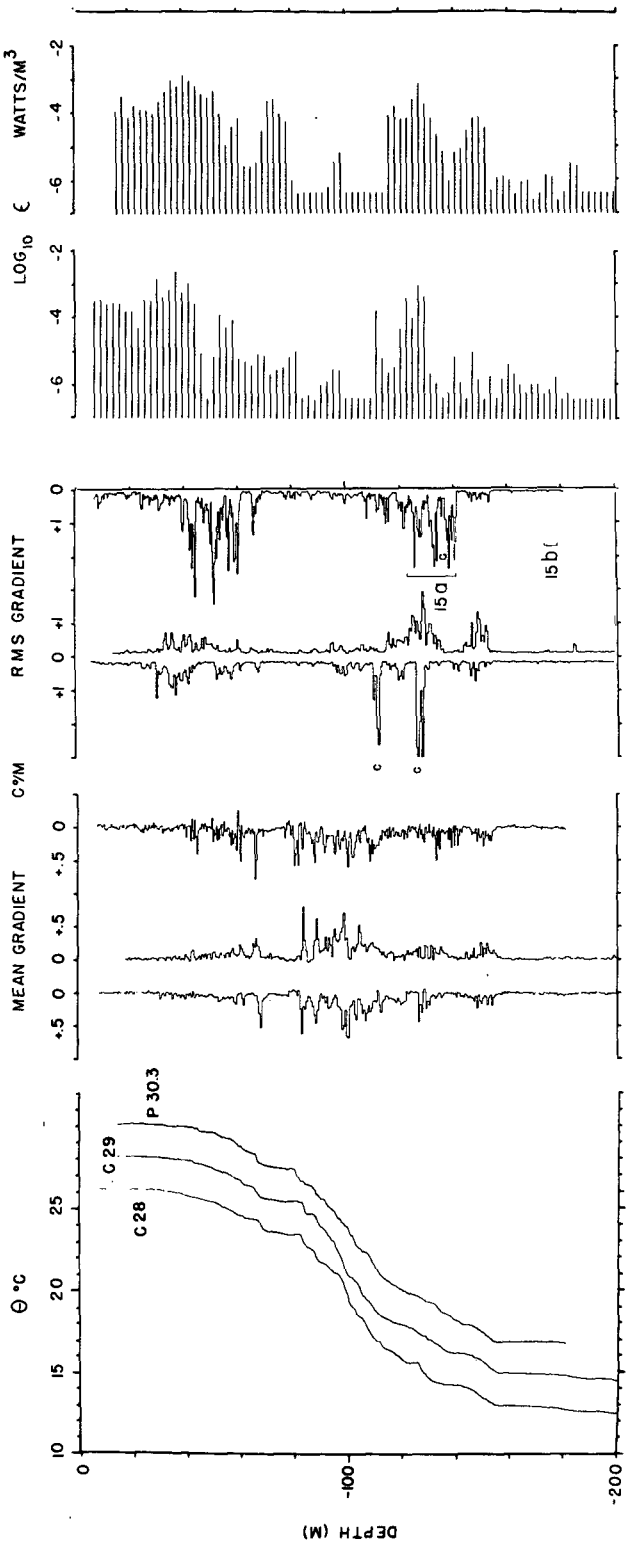

FIG. 11. Camel drop 28, Camel drop 29 and Pumpkin drop 30.

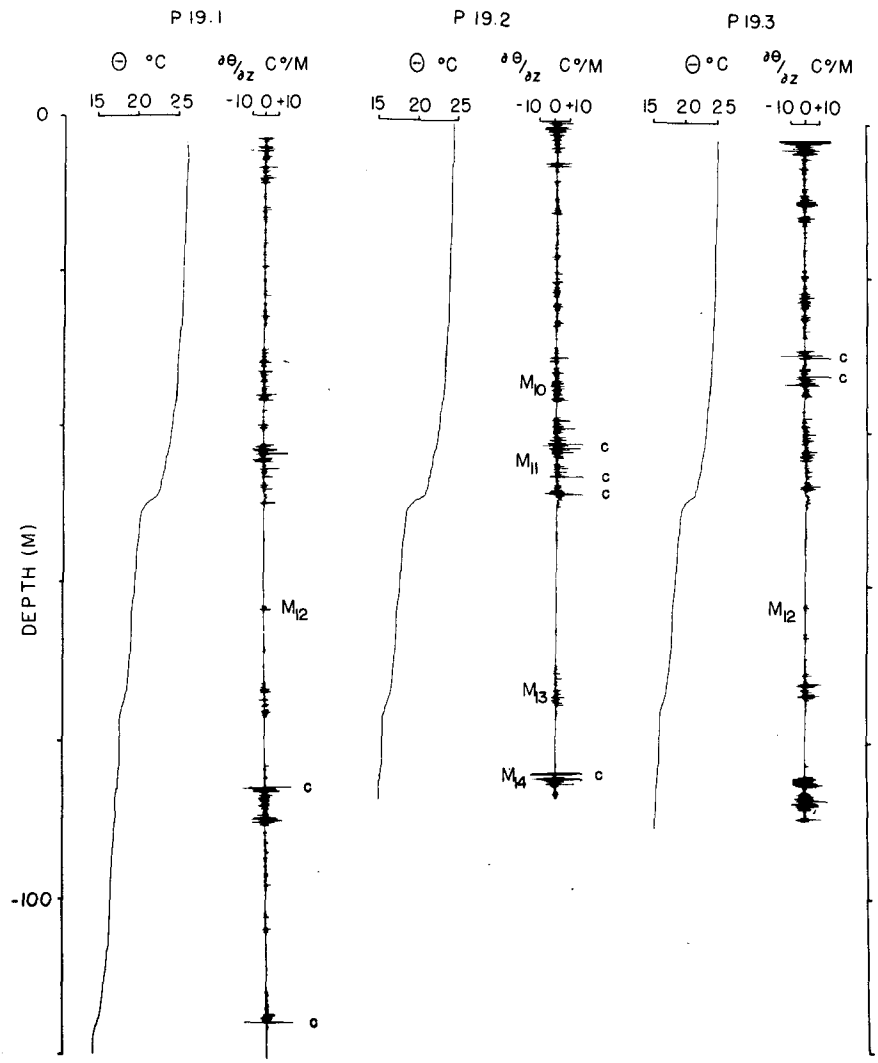

FIG. 12. Original data from Pumpkins 19.1, 19.2 and 19.3.

the thermocline. As discussed by Crawford and Osborn (1979a), this region is dominated by the turbulence associated with the shear between the South Equatorial Current and the Undercurrent. Through the core of the current, which coincides with most of the thermocline, there is a region where the temperature finestructure is more noticeable than the microstructure (60–110 m in Fig. 11). In this region the local dissipation rates are also considerably less than above. Below that region the dissipations increase and patches of large rms temperature gradient are seen.

Fig. 9 shows quite striking similarities between the microstructure profiles of the individual instruments in drops 18 and 19 which were taken more than 1 h apart. The original data are shown in Fig. 12. There is microstructure throughout the upper layer with the suggestion of two continuous patches (which have been labeled M_{10} and M_{11}) in the lower part of the upper layer. There is a thin feature, labeled M_{12} in two of the traces. Turbulent patches at M_{13} and M_{14} show in all three traces. The agreement is also striking between the Camel and the Pumpkin in the processed profile of drop 24 (Fig. 10) and in the original data traces. Fig. 13 shows the two instruments sampling similar features until the 155–145 m depth interval. In this region the Camel and Pumpkin both show a microstructure patch but the depth differs between the two samples. The feature is ~7 m shallower in the Camel data. The reason for this difference in elevation is unknown but it is unlikely to be due to instrumental effects or the depth-fitting procedure since the two profiles coincide so well over the shallower part of the drop. Other than this one feature, the two profiles are quite similar as Fig. 10 indicates. However, the signal level is considerably lower than in the other equatorial drops.

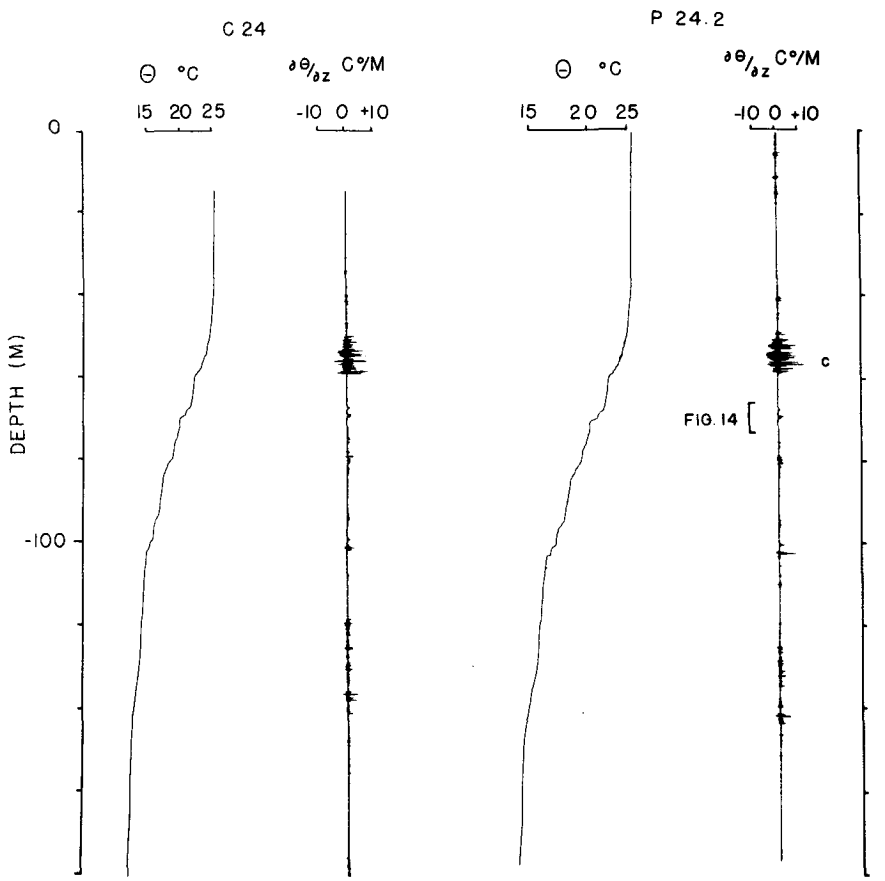

FIG. 13. Original data for Camel 24 and Pumpkin 24.2.

Note the temperature gradient through the thermocline for P24.2 which has a characteristic one-sided shape shown in Fig. 14. These gradients are without associated velocity microstructure. These features are observed in Camel profiles 23, 24, 28 and 29 in the region between 60 and 100 m. This region contains the salinity maximum and the core of the Undercurrent as located with velocity profiles (Bruce and Katz, 1976).

The three profiles (28, 29 and 30) were taken about 1 h apart and form a time series, shown in Fig. 11. One of its most interesting facets is the region between 100 and 150 m depth. The rms gradient distribution changes dramatically between the drops. The energy dissipation profiles all show a maximum between 120 and 130 m. However, the amplitude of this maximum and its vertical extent and distribution vary significantly from one drop to the next. The variations in the thermal microstructure are very large in the 130–150 m range.

The most important features for the Equatorial drops are as follows:

1) The overall temperature structure of the water column shows the spreading of the thermocline which is known to be of the Equatorial Undercurrent.

2) The finestructure as revealed by profiles of the averaged gradient presents a region with many minor temperature changes (rather than the one or two major temperature steps which were found in the other drops). This is especially noticeable in drops 28, 29 and 30.

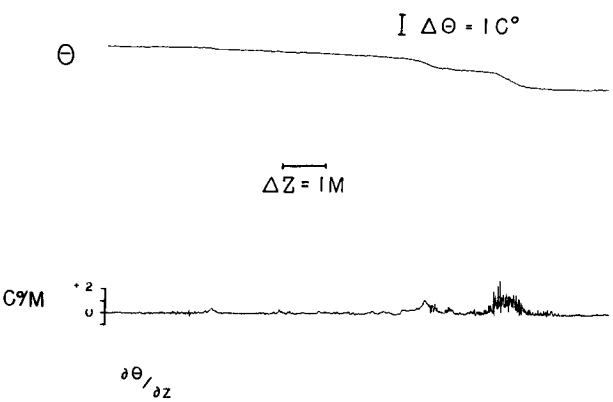

FIG. 14. Gradients through the core of the Equatorial Undercurrent from Pumpkin 24.2.

TABLE 2. Measured values of the mean temperature gradient, the temperature gradient variance and the Cox numbers for suitable profiles. Depth intervals are identified with respect to features of the local water column.

Drop	Depth interval (m)	$\frac{\partial\bar{\theta}}{\partial z}$ (C° m^{-1})	$\left(\frac{\partial\theta'}{\partial z}\right)^2$	Cox number	Relative location in the water column
19.1	4–43	5.4×10^{-2}	1.9	660	Above core
	43–52	3.9×10^{-1}	5.3	35	Core
	52–138	6.4×10^{-2}	4.6×10^{-1}	111	Below core
19.2	1–39	4.1×10^{-2}	3.3	1950	Above core
	39–52	3.0×10^{-1}	4.0	44	Core
	52–87	7.7×10^{-2}	1.0	170	Below core
19.3	5–40	4.6×10^{-2}	8.8	4200	Above core
	40–51	3.4×10^{-1}	1.2	10	Core
	51–91	6.9×10^{-2}	1.0	220	Below core
21.1	11–47	1.4×10^{-2}	6.1×10^{-3}	32	Above thermocline
	47–101	2.1×10^{-1}	8.8×10^{-1}	20	Thermocline
	101–165	1.6×10^{-2}	8×10^{-4}	3	Below thermocline
21.2	7–47	1.1×10^{-2}	7.2×10^{-3}	60	Above thermocline
	47–101	2.1×10^{-1}	6.1×10^{-1}	14	Thermocline
	101–152	1.8×10^{-2}	7.4×10^{-4}	2.2	Below thermocline
24.2	1–48	1.4×10^{-2}	9.6×10^{-2}	500	South Equatorial Current
	48–58	2.0×10^{-1}	7.1	180	Shear region
	58–108	1.4×10^{-1}	7.6×10^{-2}	3.7	Core
	108–165	3.7×10^{-2}	4.2×10^{-2}	31	Shear region
30.3	36–60	5.8×10^{-2}	3.8	1100	Shear region
	60–77	7.5×10^{-2}	1.5×10^{-1}	26	Core
	77–109	1.7×10^{-1}	5.1×10^{-2}	1.7	Core
	109–121	1.2×10^{-1}	1.8×10^{-1}	13	Shear region
	121–142	8.7×10^{-2}	2.1	280	Shear region
	142–181	2.8×10^{-2}	1.1×10^{-2}	14	Below undercurrent

3) The microstructure gradient variance intensities are significantly lower within the thermocline than outside of it. This is also true of energy dissipation.

4) The transition between the upper layer and the thermocline is more gradual than in the other profiles and it is accompanied by high-energy dissipation and microstructure gradient variance.

5) Again, microstructure patches generally appear continuously between different instrument profiles.

4. Discussion

a. Cox numbers

Table 2 gives the depth range, mean gradient, mean-square gradient and Cox number C, where

$$C = \overline{\left(\frac{\partial\theta'}{\partial z}\right)^2} \Big/ \left(\frac{\overline{\partial\theta}}{\partial z}\right)^2.$$

Blocks of 2048 points were Fourier transformed, spectrally corrected and averaged in groups of eight adjacent frequency bands; adjacent spectra were then averaged together to cover the depth interval.

The correction of the data for the thermistor response results in considerably higher gradient variances in regions of intense temperature fluctuations, e.g., drops 19.1, 19.2 and 19.3 from 40 to 50 m, where the mean-square value as shown in Table 2 is much larger than would be expected from Fig. 9. The error in the values in Table 2 is difficult to estimate for it is mostly associated with the correction for the thermistor and the clipping of peak values with some contribution to the correction of the electronics. Thus the percentage error is dependent upon the signal's level. It was not originally anticipated that the data from the instruments would be corrected for thermistor response without the noise dominating the corrected spectra. However, near the Equatorial Undercurrent the temperature gradient variance is so large that the noise level of the instrument is not the limiting factor. Fig. 15a shows the corrected and uncorrected spectra for drop 30.3 122 to 142 m. Fig. 15b shows the spectra for a quieter region, drop 30.3 174 to 178 m. (Note: both axes on each plot are linear but the vertical scales differ by 10^2 between the graphs.) These locations are marked on Fig. 11. Thus rather than give an error estimate we will state that the uncertainty on the low-frequency gradient calibrations is $\pm 10\%$ and the thermistor correction and the clipping effect are such as to make the variance estimates here more likely to be underestimates than overestimates.

The result that emerges from the Cox numbers is consistent with the velocity microstructure measurement of high dissipation and diffusion in the shear region above the core, relatively low diffusion due to low turbulence levels through the core and another lesser maximum in turbulence in the shear region below the core. This picture is similar to that of Gregg (1976) although the Cox numbers are often higher for a given region of the current system.

The variability in Cox numbers over comparable intervals can be seen by comparing the results for drops 19, 24 and 26. There is a large variation above the core in drop 19 associated more with differences in the mean-square gradient than with differences in the averaged gradient. In the shear region below the core in drop 19 the Cox number varies by a factor of 2 between the three profiles, again due to the difference in the thermal microstructure.

The Cox number values below the thermocline in drops 21.1 and 21.2 are low and all the mean-square-gradient values at this station are on the low side of the range of values observed in the Undercurrent.

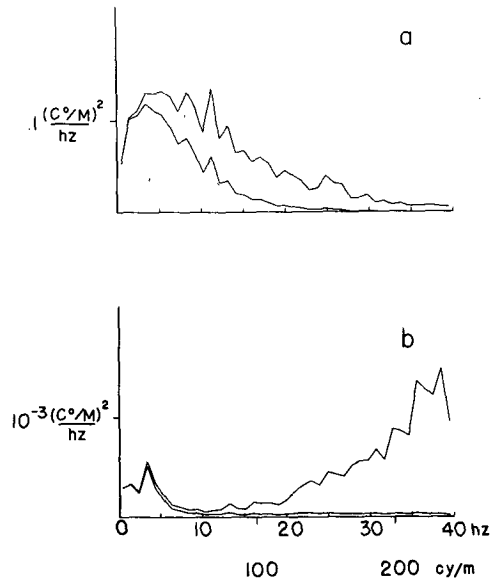

FIG. 15. Spectrum of data from 122–142 m (a) and from 174–178 m (b), both drop 30.3. These spectra are plotted with linear scales on both axes. Note that the scale changes by a factor of 100 between the two plots.

b. Comparison with Pacific data

There are interesting differences between the temperature microstructure data presented in this paper and that reported for the Pacific Equatorial Undercurrent by Gregg (1976). His measurements are close to the Equator at 155°W. The data drops each cover a 150 m depth interval, with drops extending as deep as 500 m. His data are shown as 0.5 m averages of temperature, temperature gradient and rms temperature gradient, and are thus directly comparable to the data in this paper. We will restrict our attention to the Pacific data above 200 m depth which would include the core of the current. The values for the 0.5 m averages of the gradient in the Pacific are much lower than in the Atlantic; Gregg's two largest values are ~ 0.6 C° m^{-1} and 0.3 C° m^{-1}. However, his mean temperature gradient data is averaged with a five-point cosine filter. Near the Equator in the Atlantic the data show values up to and exceeding 1.5 C° m^{-1} (P19.2, Fig. 9) which when these are cosine filtered the peak value is 0.9 C° m^{-1}. The gross mean gradient below the mixed layer is larger in the Atlantic with a decrease of ~ 10 C° between 60 and 130 m (Fig. 11), and of 6 C° between 37.5 and 75 m depth in Fig. 9. The average gross gradient is 1.5×10^{-1} C° m^{-1}. These values compare with 6 C° between 80 and 140 m and 7 C° between 80 and 160 m in Gregg's Figs. 4a and 4b for an average gross gradient of 9.4×10^{-2} C° m^{-1}. Thus the gross gradients are $\sim 50\%$ greater in our data for the Atlantic than in Gregg's data for the Pacific.

Levels of the gradient variance (and thus the rms gradient) are also higher in the Atlantic data. Values up to 3.5 C° m^{-1} are seen in Figs. 9 and 11, with many regions showing values in excess of 1 C° m^{-1}. The Pacific data of Gregg (which are not cosine filtered) show a maximum value for the average over 0.5 m of 1 C° m^{-1} with the next largest value again about half as large. The Atlantic values differ from the Pacific values by more than the simple ratio of the gross temperature gradients.

Certainly, part of the explanation for the higher gradient levels is associated with the large-scale vertical temperature gradient being larger in the equatorial Atlantic. However, the ratio of the half-meter average of the gradients between the two oceans is larger than the ratio of the large-scale mean gradients. Part of the explanation is likely associated with the fact that the Undercurrent is shallower in the Atlantic than in the Pacific, producing a large mean shear. Unfortunately, we have no information about the velocity profile in the Pacific associated with Gregg's measurement. Thus we cannot assess the difference in the mean velocity shear between the two sets of measurements.

5. Summary

1) The regions of high-wavenumber temperature gradient fluctuations that are normally called microstructure are related to velocity turbulence fluctuations.

2) When the temperature gradient microstructure

is consistently of one sign no associated velocity microstructure is found.

3) The patches in the equatorial region seem to be contiguous over distances of several tens of meters horizontally. We do not have data for longer separations.

4) Some numerical values for the Cox number are now available. The repetitive sampling with multiple instruments also indicates the variability associated with these values.

5) The temperature microstructure and the temperature finestructure are more intense in these measurements in the Atlantic than in Gregg's measurements in the Pacific. More work is appropriate to see if there is a difference in the level and/or nature of the turbulence between the two equatorial regimes. The problem of temporal and spatial variation of microstructure should be attached in conjunction with a well resolved mean field. Perhaps the equatorial regions with their large shear are unique "laboratories" due to their large mean shears.

REFERENCES

Bruce, J. G., and E. J. Katz, 1976: Observations in the equatorial Atlantic during GATE, June and July 1974, from *Atlantis* II. Woods Hole Oceanographic Institution, Tech. Rep. WHOI-76-54, 156 pp.

Crawford, W. R., and T. R. Osborn, 1979a: Microstructure measurements in the Atlantic Equatorial Undercurrent during GATE. *Deep-Sea Res.* (in press).

——, and ——, 1979b: Energetics of the Atlantic Equatorial Currents. *Deep-Sea Res.* (in press).

Gargett, A. E., 1976: An investigation of the occurrence of oceanic turbulence with respect to finestructure. *J. Phys. Oceanogr.*, **6,** 139–156.

Gregg, M. C., 1976: Temperature and salinity microstructure in the Pacific Equatorial Undercurrent. *J. Geophys. Res.*, **81,** 1180–1196.

——, 1977: Variations in the intensity of small-scale mixing in the main thermocline. *J. Phys. Oceanogr.*, **7,** 436–454.

——, and C. S. Cox, 1971: Measurements of the oceanic microstructure of temperature and electrical conductivity. *Deep-Sea Res.*, **18,** 925–934.

——, —— and P. W. Hacker, 1973: Vertical microstructure measurements in the central North Pacific. *J. Phys. Oceanogr.*, **3,** 458–469.

Lueck, R. G., O. Hertzman and T. R. Osborn, 1977: The spectral response of thermistors. *Deep-Sea Res.*, **24,** 951–970.

Osborn, T. R., 1977: The design and performance of free-fall microstructure instruments at the Institute of Oceanography, University of British Columbia. IOUBC Ms. Rep. No. 30, 31 pp.

——, 1978: Measurements of energy dissipation adjacent to an Island. *J. Geophy. Res.*, **83,** 2939–2957.

——, and C. S. Cox, 1972: Oceanic fine-structure. *Geophys. Fluid Dyn.*, **3,** 321–345.

Thorpe, S. A., 1971: Experiments on the instability of stratified shear flow: miscible fluids. *J. Fluid Mech.*, **46,** 299–319.

Woods, J. D., 1968: Wave-induced shear instability in the summer thermocline. *J. Fluid Mech.*, **32,** 791–800.